J Solid State Electrochem (2009) 13:713–720
DOI 10.1007/s10008-008-0595-2

ORIGINAL PAPER

Preparation and growth behavior of amorphous $Pd_{40}Ni_{40}P_{20}$ film by electrodeposition

Y. Xu · X. M. Ge · J. Z. Jiang

Received: 3 March 2008 / Accepted: 19 May 2008 / Published online: 24 June 2008
© Springer-Verlag 2008

Abstract Amorphous $Pd_{40}Ni_{40}P_{20}$ alloy has potential applications in electronics and catalytic industry. In this paper, amorphous $Pd_{40}Ni_{40}P_{20}$ films were prepared by electrodeposition. Samples were characterized by scanning electron microscopy, energy dispersive X-ray spectroscopy, transmission electron microscopy, X-ray diffraction, and profilometry. Voltammetric curves and potential–time transient indicate the leading role of Pd in the initial growth stage. Based on compositional, morphological, and electrochemical analyses, $Pd_{40}Ni_{40}P_{20}$ electrodeposition is regarded as Pd-induced PdNiP co-deposition accompanying with hydrogen evolution reactions.

Keywords Electrodeposition · $Pd_{40}Ni_{40}P_{20}$ · Amorphous film · Growth behavior

Introduction

$Pd_{40}Ni_{40}P_{20}$ is one of the earliest metallic glasses [1, 2], which has been intensively studied due to its compositional simplicity and large glass-forming ability [3, 4]. Most studies of $Pd_{40}Ni_{40}P_{20}$ focus on ribbon and ingot samples. Amorphous thin films, usually having unique surface and confinement effects [5], should be of theoretical and experimental interest to study the thermodynamic and structural differences between $Pd_{40}Ni_{40}P_{20}$ film and the bulk counterpart. Furthermore, due to high wear and corrosion resistances, PdNi, NiP, and PdP alloys have various applications. For example, PdNi could be used as contact layer to replace Au in electronics [6] and electrode for hydrogen evolution reaction (HER) and oxidation [7–9] and anode in methanol oxidative fuel cells [10]. NiP is widely used as catalytic material [11], and PdP is also used as cathodes for oxygen reduction [12]. Corrosion resistance of electrodeposited metal–metal binary alloys can be enhanced by alloying with P [13–15], and the catalytic performance of PdP and NiP alloys can be improved by incorporating Ni [16] and Pd [17], respectively. $Pd_{40}Ni_{40}P_{20}$, the alloy with strong glass-forming ability in PdNiP system, could have many potential applications in electronic [18], energy [19], and catalytic [17] industries.

Electrochemical deposition (electrodeposition) is a simple and effective way to synthesize metallic films. Many metal-phosphorus plating systems have been developed after the discovery of amorphous NiP [20]. Masaki et al. [18] reported the PdNiP electrodeposition patent in 1992. Their films are crystalline, and P is not more than 10 at.%. In the present work, amorphous $Pd_{40}Ni_{40}P_{20}$ films are electrodeposited from an additive-free electrolyte with complexing agent. The electrolyte is derived from NiP [11], PdP [12, 21, 22], and PdNi [9, 10, 23] systems. Effects of various plating conditions on structure and morphology of $Pd_{40}Ni_{40}P_{20}$ films are investigated. The growth behavior during $Pd_{40}Ni_{40}P_{20}$ electrodeposition is discussed.

Experimental

PdNiP films were deposited from conventional three-electrode glass cell. Galvanostatic electrodeposition was controlled by

Y. Xu · J. Z. Jiang (✉)
International Center for New-Structured Materials (ICNSM), Zhejiang University and Laboratory of New-Structured Materials, Hangzhou 310027, People's Republic of China
e-mail: jiangjz@zju.edu.cn

Y. Xu · J. Z. Jiang
Department of Materials Science and Engineering, Zhejiang University, Hangzhou 310027, People's Republic of China

X. M. Ge
Fuel Cells and Energy Research Lab 1, School of Mechanical and Aerospace Engineering, Nanyang Technological University, 50 Nanyang Avenue, Singapore 639798, Singapore

CHI 1140 electrochemical analyzer (CH Instruments). All chemicals in this work were of reagent grade. Plating electrolyte and operating conditions are listed in Table 1. Bath temperature was controlled by either thermostat or ice water bath. The pH value of electrolyte was adjusted by adding dilute NaOH and HCl. Working electrode was mechanically polished Cu plate (99.5%) with root-mean-square roughness of 5 nm, which was measured by atomic force microscopy (Seiko Instruments, SPI 3800N). Counter and reference electrode were platinum plate and saturated calomel electrode, respectively.

Film morphology and composition were characterized by field emission scanning electron microscopy (SEM, SIRION-100, FEI) with energy dispersive X-ray spectroscopy (EDX, Genenis 4000X). Melt-spun $Pd_{40}Ni_{40}P_{20}$ ribbons were used to calibrate the EDX measurement. For transmission electron microscopy (TEM; Hitachi H-9000NAR) observation, standing-free PdNiP films were prepared by substrate stripping in chromic acid solutions. X-ray diffraction (XRD) measurements were performed on a Thermo ARL X'Tra diffractometer with Cu Kα radiation. Film thickness was measured by profilometer (Sloan Dektak III).

Cyclic voltammetric (CV) curves were acquired from CHI 604B electrochemical work station (CH Instruments). Potential range was from −0.10 to −1.60 V, and the scan rate was 5 mV/s. Potentiostatic electrodeposition is performed at CHI 1140 using amperometric I–time curve mode.

Results and discussion

Quantitative compositions of PdNiP films were measured. Figure 1 shows EDX spectra of standard $Pd_{40}Ni_{40}P_{20}$ ribbon and film with nominal composition $Pd_{41.1}Ni_{38.8}P_{20.1}$. Compositions of both samples were calculated from Ni K, Pd L,

Table 1 Plating conditions for PdNiP electrodeposition

Plating conditions	Values
Electrolyte	
$PdCl_2$	0.01~0.02 (0.01)[a] mol/l
$NiSO_4 \cdot 6H_2O$	9~13 (10)[a] g/l
$H_2NCH_2CH_2NH_2$	0.09~0.12 (0.096)[a] mol/l
H_3PO_3	15~30 (20)[a] g/l
H_3BO_3	20 g/l
Operating conditions	
Bath temperature	5°C
pH	1.3~2.00 (1.70)[a]
Current density	8~18 (12.5)[a] mA/cm^2
Growth time	10~300 (300)[a] s
Substrate	Copper

[a] Parameters in the parentheses are for $Pd_{40}Ni_{40}P_{20}$ deposition

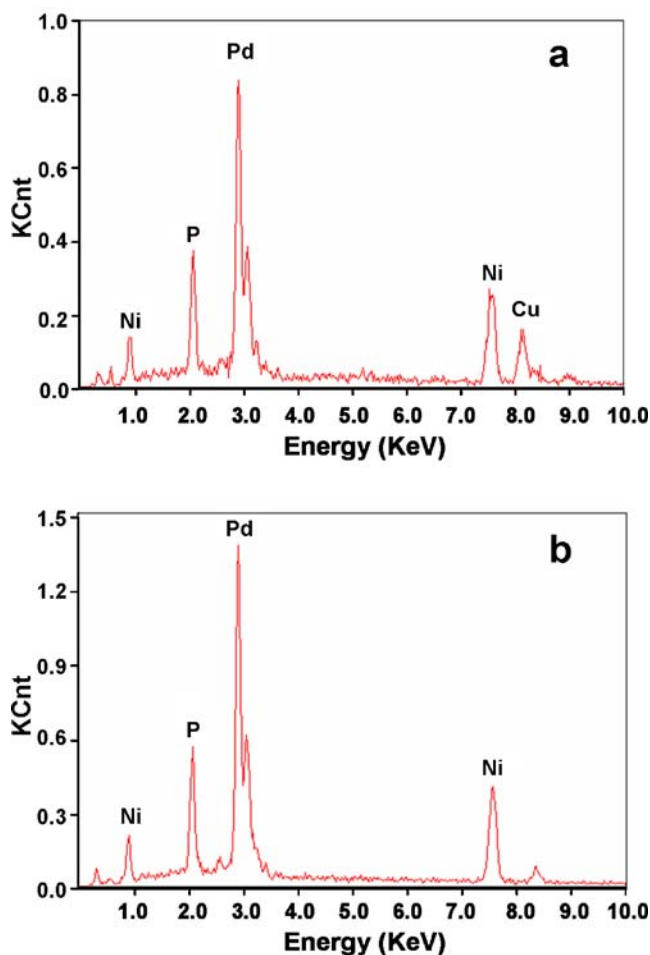

Fig. 1 EDX spectra of **a** electrodeposited $Pd_{41.1}Ni_{38.8}P_{20.1}$ film on Cu substrate; **b** standard melt-spun $Pd_{40}Ni_{40}P_{20}$ ribbon

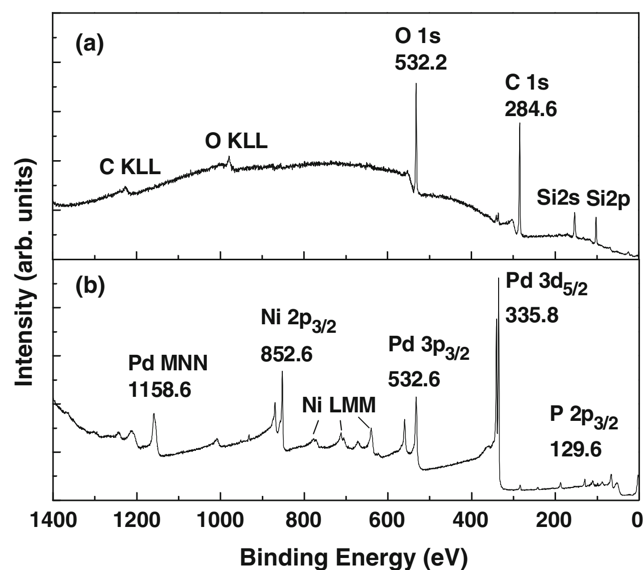

Fig. 2 X-ray photoelectron spectra of $Pd_{40}Ni_{40}P_{20}$ films. **a** As-deposited and **b** after 3 min Ar sputtering

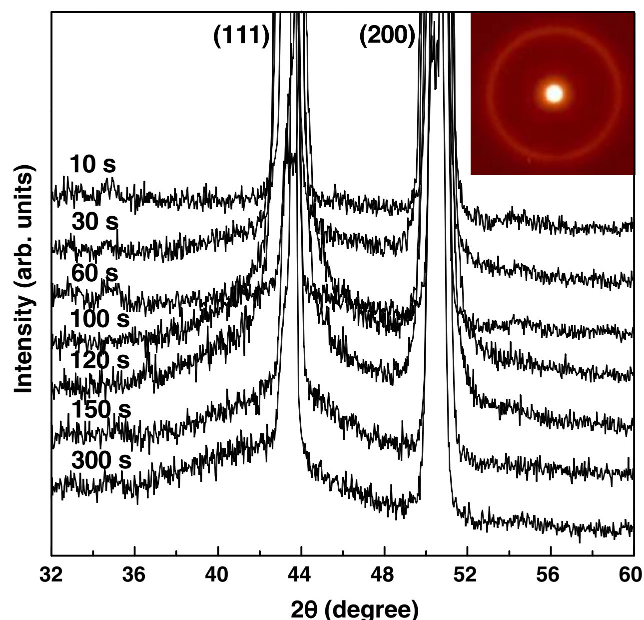

Fig. 3 XRD patterns of electrodeposits prepared from $Pd_{40}Ni_{40}P_{20}$ electrolyte on Cu substrate. The inset shows SAED patterns of a certain PdNiP film

and P K lines. The two spectra are almost identical, except Cu lines (from sample holder) superimpose on the $Pd_{41.1}Ni_{38.8}P_{20.1}$ spectrum. Cu backgrounds are inevitable, as the films are much thinner than the electron impact zone during EDX measurement. Trace of C and O peaks near 0.3 and 0.5 keV were detected at both spectra [24], which can be attributed to surface contamination. Actually, X-ray photoelectron spectroscopy analysis confirmed the metallic nature of the film after Ar sputtering for 3 min in Fig. 2. The binding energies of Pd $3d_{5/2}$, Ni $2p_{3/2}$, and P $2p_{3/2}$ are the same between as-deposited film and ribbon $Pd_{40}Ni_{40}P_{20}$ alloys [25].

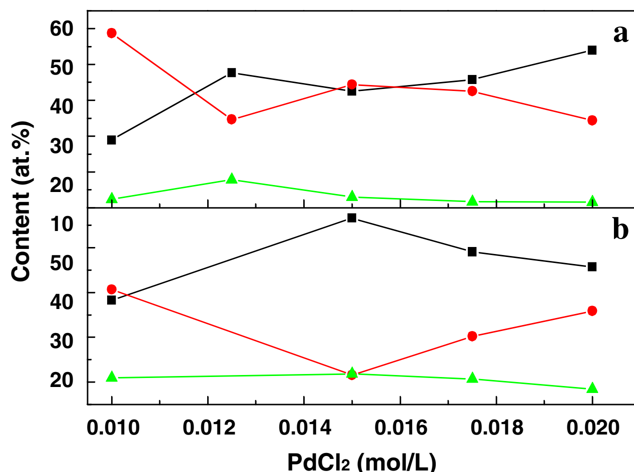

Fig. 5 Effect of $PdCl_2$ concentration on film composition. Plating conditions are according to $Pd_{40}Ni_{40}P_{20}$ electrolyte except pH value: **a** pH=2.00; **b** pH=1.50. Pd (*square*); Ni (*circle*); P (*triangle*)

Film structures are characterized by XRD and TEM. Although peaks from Cu substrate exist in the XRD patterns due to thin film effect, a broad diffraction peak is observed below the substrate (111) peak, especially after 100 s deposition

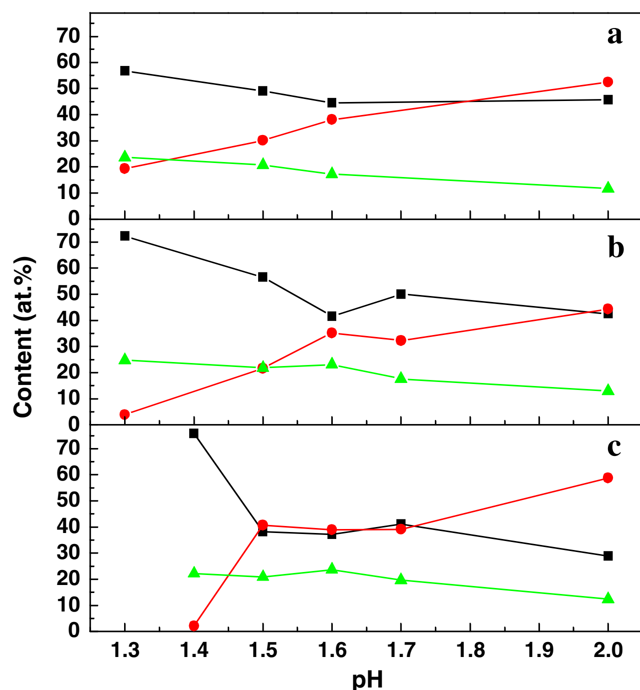

Fig. 4 Effect of pH value on film composition. Plating conditions are according to $Pd_{40}Ni_{40}P_{20}$ electrolyte except $PdCl_2$ concentration: **a** $PdCl_2$ 0.0175 mol/l; **b** $PdCl_2$ 0.015 mol/l; **c** $PdCl_2$ 0.01 mol/l. Pd (*square*); Ni (*circle*); P (*triangle*)

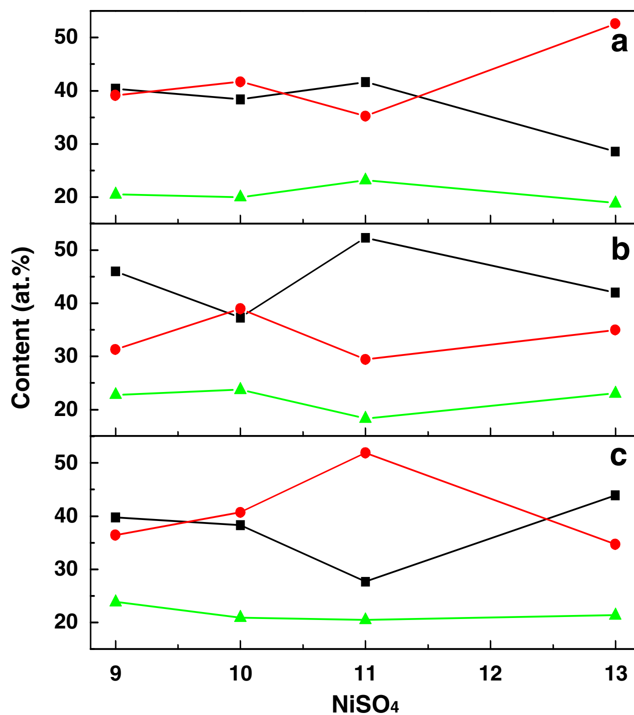

Fig. 6 Effect of $NiSO_4{\cdot}6H_2O$ concentration on film composition. Plating conditions are according to $Pd_{40}Ni_{40}P_{20}$ electrolyte except pH value: **a** pH=1.70; **b** pH=1.60; **c** pH=1.50. Pd (*square*); Ni (*circle*); P (*triangle*)

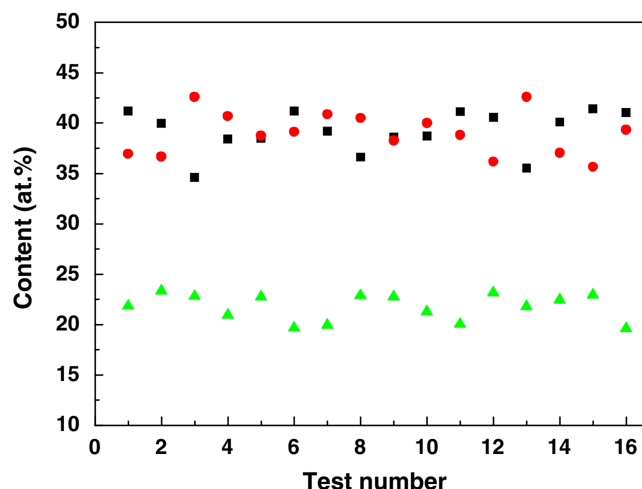

Fig. 7 Reproducibility of $Pd_{40}Ni_{40}P_{20}$ electrodeposition. Pd (*square*); Ni (*circle*); P (*triangle*)

(Fig. 3). The films are absent with distinct contrasts in TEM images (not shown here), and their electron diffraction patterns exhibit diffusive halos (inset of Fig. 3). These results confirm the amorphous nature of the deposited $Pd_{40}Ni_{40}P_{20}$ films.

The pH value and concentrations of $PdCl_2$ and $NiSO_4{\cdot}6H_2O$ were three key factors on compositions of the deposited films, as shown in Figs. 4, 5, and 6. Film contents are sensitive to pH value below 1.5 (Fig. 4). As the dissociation constant of ethylenediamine (en) is closely related to pH [26, 27] and pH value affects the extent of metal hydrolysis [28], reduction rates of different metal complexes are influenced by pH value. Thus, it is reasonable that the Pd/Ni atomic ratio in deposited films is not the same when we prepared them in electrolytes of different pH values. In our case, $Pd(en)_2^{2+}$ seems easier to be reduced than $Ni(en)_x^{2+}$ [i.e., $Ni(en)^{2+}$, $Ni(en)_2^{2+}$, $Ni(en)_3^{2+}$, etc.] [29] in the low pH range (below 1.5). In the middle pH range between 1.5 and 1.7, the reduction of $Pd(en)_2^{2+}$ and $Ni(en)_x^{2+}$ is comparable, thus resulting in a relative stable concentration of both Ni and Pd in films (Fig. 4c). In the high pH range (above 1.8), $Ni(en)_x^{2+}$ reduction is activated and $Pd(en)_2^{2+}$ reduction is inhibited relatively. P content of the films decreases with increasing pH value (Fig. 4), which coincides with NiP electrodepositions [30, 31]. To reach P content of about 20 at.% in the deposited films, it is found that a “pH window” of 1.5~1.7 should be used (Figs. 4, 5, and 6). The effect of electrolyte concentration on composition of films is negligible from Figs. 5 and 6. When $PdCl_2$ increases from 0.01 to 0.025 mol/l and $NiSO_4{\cdot}6H_2O$ increases from 9 to 13 g/l, film composition varies slightly. Table 1 summarizes the plating conditions for PdNiP electrodeposition. The reproducibility of $Pd_{40}Ni_{40}P_{20}$ film synthesis is estimated to be about 80% with a tolerance of 3 at.% concentration fluctuation (Fig. 7). The thickness of the films is about 200 nm, which was tested by Sloan Dektak III profilometer.

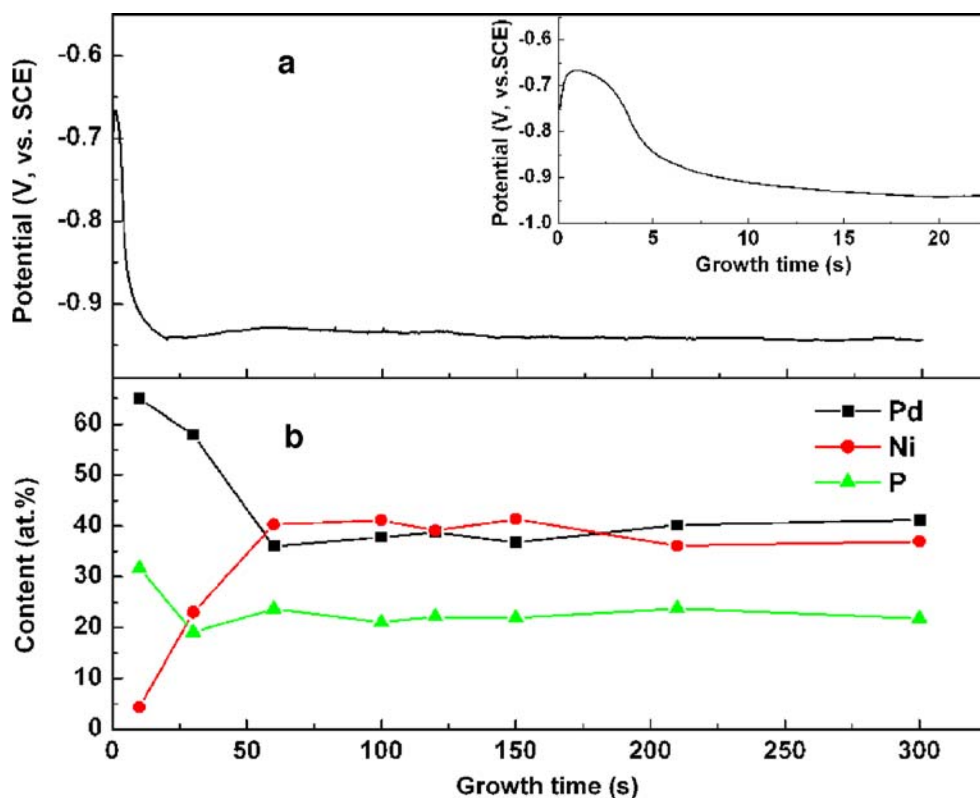

Fig. 8 **a** Potential–time transient for $Pd_{40}Ni_{40}P_{20}$ electrolyte. The *inset* shows curve in a time range of 0–25 s. **b** Compositions of PdNiP deposits with different growth times. Plating conditions are according to $Pd_{40}Ni_{40}P_{20}$ electrolyte

Potential–time transient in Fig. 8a delineates the whole depositing process of $Pd_{40}Ni_{40}P_{20}$ films, and the composition evolution of the film during the electrodepositing process (within 10~300 s) is shown in Fig. 8b. It is worth noting that the grow rate is different between initial and saturated growth stages. In the initial growth period, Pd content is dominant in the deposited films. Nanopores were detected on film surface, as marked by arrows in Fig. 9a. Nanopores are located along scratches on Cu substrate, where small hydrogen bubbles coalesce into large bubbles when they can not escape from the scratches simultaneously. Based on naked-eye observation, hydrogen bubbles escape more easily on PdNiP surface than on Cu substrate. Therefore, nanopores in Fig. 9a are the remnant of large hydrogen bubbles on the scratches. Larger nanopores with a size of 48±11 nm are detected around the film surface with growth time of 30 s (Fig. 9b). More studies are still required to understand the nature of deposition in the initial period. While the deposition time increases, the system reaches stable growth stages: concaves (former nanopore sites) fade away, and the surface is composed of distinct nodules with diameter of 90±24 nm (Fig. 9c). Film composition saturates for deposition times longer than 60 s. For films with growth time up to 300 s, smooth and diffusive nodules finally cover the whole surface (Fig. 9d). Morphology evolution during $Pd_{40}Ni_{40}P_{20}$ deposition is illustrated in Fig. 9e.

Cyclic voltammetry analysis was performed for further description of the initial growth stage. Figure 10 shows the CV curves of H_2SO_4, H_3PO_3 + H_3BO_3, NiP, PdP, and PdNiP electrolytes. In different potential ranges, shoulders are observed for H_3PO_3+H_3BO_3, NiP, PdP, and PdNiP curves. To investigate reaction processes at different potentials, potentiostatic depositions were performed on NiP, PdP, and PdNiP electrolytes (Table 2). Almost the same composition of deposited films were detected for NiP films depositing at −0.9, −1.1, and −1.4 V and PdP films depositing at −0.58, −0.7, and −0.92 V. These results indicate that deposition behaviors above and below shoulders in Fig. 10 for NiP and PdP CV curves are similar. For PdNiP film, it is found that at −0.58 V, the film contains only Pd and P while no Ni element was detected in the film. At −0.72 V, about 1.8 at.% Ni was detected in the film, while the film prepared at −0.92 V contains about 23.7 at.% Ni. Thus, Ni reduction competes

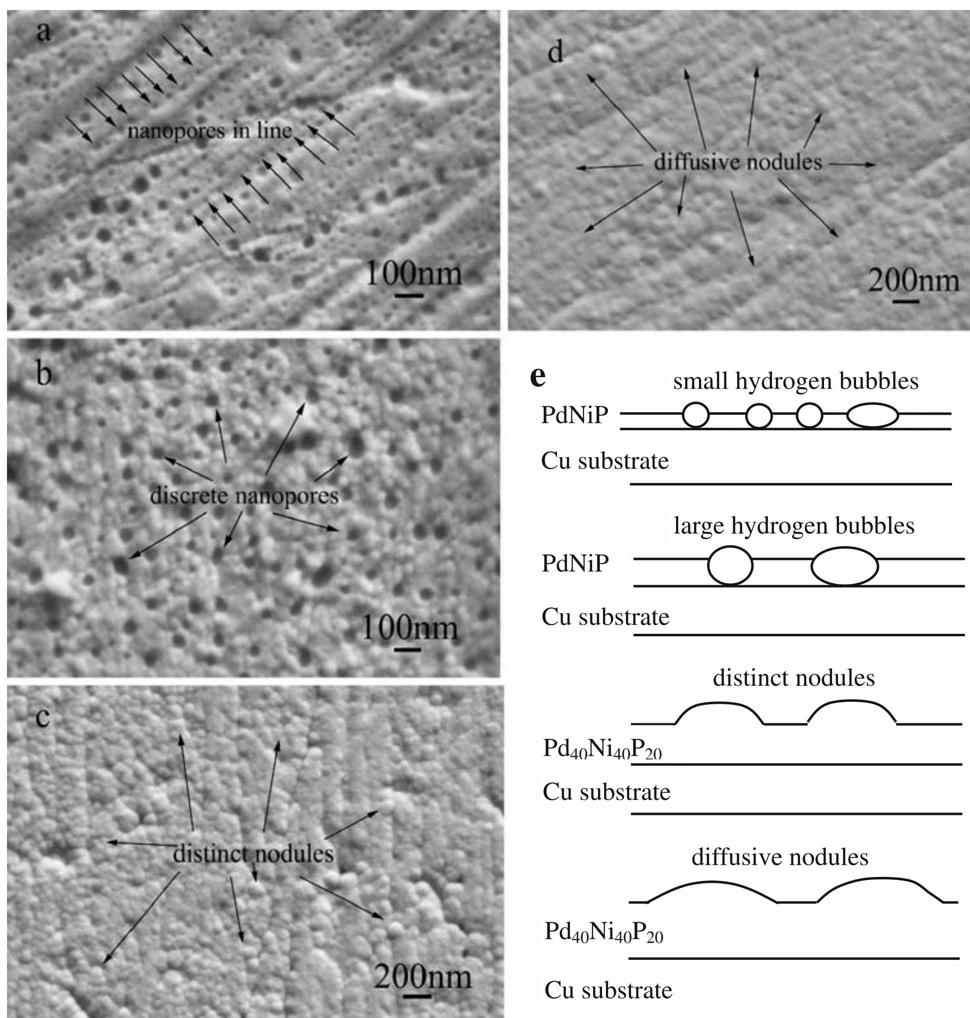

Fig. 9 Field emission SEM images of films deposited from $Pd_{40}Ni_{40}P_{20}$ electrolyte with growth times **a** 10 s; **b** 30 s; **c** 60 s; **d** 120 s. **e** An illustration of morphology evolution from **a** to **d**

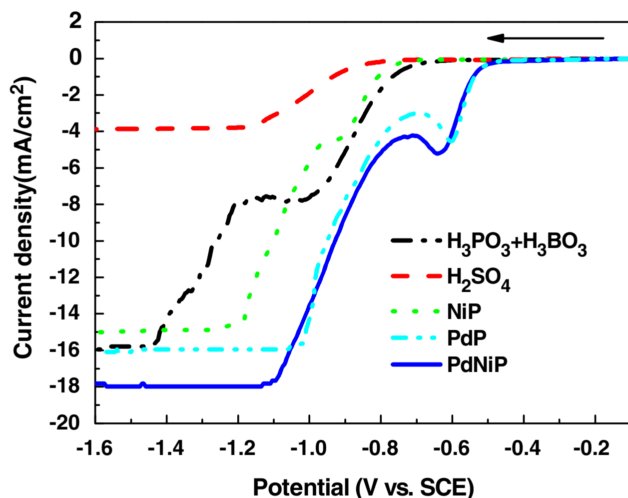

Fig. 10 Voltammetric responses of cathodic reactions for electrolytes of PdNiP ($Pd_{40}Ni_{40}P_{20}$ electrolyte in Table 1), PdP ($Pd_{40}Ni_{40}P_{20}$ electrolyte without $NiSO_4 \cdot 6H_2O$), NiP ($Pd_{40}Ni_{40}P_{20}$ electrolyte without $PdCl_2$), $H_3PO_3+H_3BO_3$ ($Pd_{40}Ni_{40}P_{20}$ electrolyte without ethylenediamine, $PdCl_2$, and $NiSO_4 \cdot 6H_2O$) and H_2SO_4. The pH values of all these electrolytes were kept to be 1.70. Scan rate is 5 mV/s. Bath temperature is 5°C. *Arrow* shows the direction of polarization

against Pd reduction after −0.72 V. The initial reduction behavior of PdNiP electrolyte is almost identical to PdP electrolyte in Fig. 10, though its peak slightly shifts to −0.64 V [−0.61 V for PdP electrolyte, which is close to the standard reduction potential of $Pd(en)Cl_2$] [32]. This peak shift results from the beginning of Ni reduction. In the curves ranging from −0.45 V to −0.64 V (−0.61 V) for PdNiP (PdP), Pd nucleates and grows rapidly [33], which induces P co-depositing and HER. HER is predominant during this stage, resulting in local depletion of Pd and proton. In contrast, buffering effects of H_3PO_3 and H_3BO_3 and stirring effect of hydrogen bubble can alleviate the local depletion. Thus, these balanced effects contribute to diffusion-limited reaction process, resulting in a limited current density of about 18 mA/cm^2 for PdNiP electrolyte.

Table 2 Film composition of potentiostatic NiP, PdP and PdNiP electrodepositions

Electrolyte	Potential (V)	Depositing time (s)	Film Compositions
NiP	0.9	2,100	$Ni_{65.5}P_{34.5}$
	1.1	1,600	$Ni_{68.6}P_{31.4}$
	1.4	500	$Ni_{67.4}P_{32.6}$
PdP	0.58	2,000	$Pd_{78.1}P_{21.9}$
	0.7	600	$Pd_{77.6}P_{22.4}$
	0.92	600	$Pd_{77.1}P_{22.9}$
PdNiP	0.58	1,200	$Pd_{76.5}P_{23.5}$
	0.72	1,200	$Pd_{75.2}Ni_{1.8}P_{23.0}$
	0.92	800	$Pd_{54.6}Ni_{23.7}P_{21.7}$

In the beginning of the galvanostatic electrodeposition in $Pd_{40}Ni_{40}P_{20}$ electrolyte, it was detected that the potential increases rapidly within 1 s (inset of Fig. 8a), which corresponds to the peak (−0.64 V) of PdNiP curve in Fig. 10. Together with the results of CV analysis, this phenomenon can be attributed to the overpotential reduction of HER, as the overpotential of HER on Pd surface is much lower than that on Cu or Ni surface [34]. As discussed before, Pd content is dominant in PdNiP films at the initial deposition stage (Fig. 8b). With such initial Pd layers, the potential shifts positively to maintain the fixed current density if we note that current efficiency is only 15% in the PdNiP system. As growth time increases, the potential shifts rapidly to negative direction because of double-layer charging effect [35]. Potential–time transient are consistent with CV curves. For potential–time transient of $Pd_{40}Ni_{40}P_{20}$ electrolyte, the electrolysis potential saturates at −0.94 V, while for CV curve, it corresponds to −0.97 V (Fig. 10). No abrupt potential drop is observed in the time ranging from 20–300 s

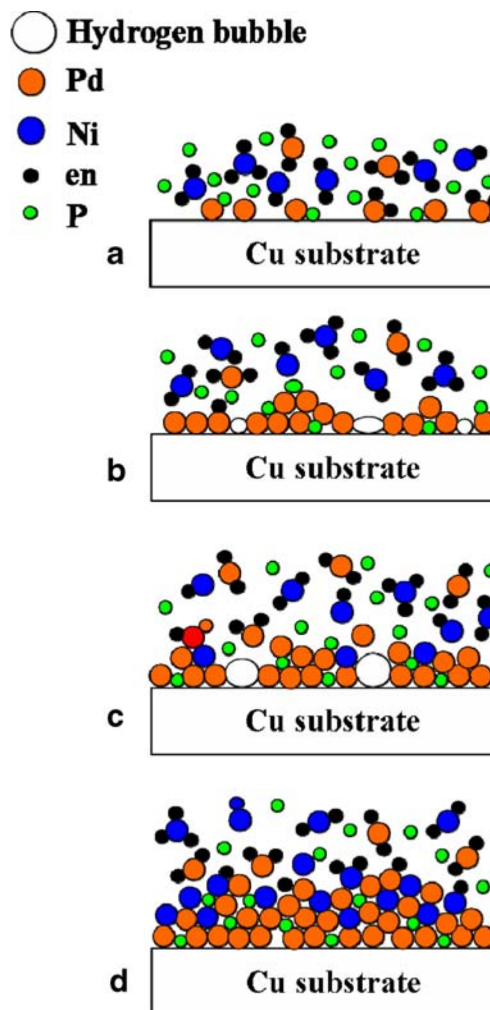

Fig. 11 Schematics of surface evolution during $Pd_{40}Ni_{40}P_{20}$ electrodeposition

[36]. This is quite different with conventional low concentration [33] or simple metal [37] electrodeposition, which exhibit potential fluctuation with increasing times. It indicates that the $Pd_{40}Ni_{40}P_{20}$ galvanostatic electrodeposition process is most likely reaction-rate controlled because the current density 12.5 mA/cm^2 is used, which is less than the limited current density 18 mA/cm^2 in Fig. 10. Note that we could not completely rule out the possibility for a partial mass-transfer-controlled process in the present deposition because for multi-component system, the mechanism can be tricky and some steps can be mass-transport controlled even for low current compared to the limited diffusion current. More investigations, e.g., impedance spectroscopy experiments, are required to clarify this issue.

In general, a schematic illustration of surface evolution during $Pd_{40}Ni_{40}P_{20}$ electrodeposition is given in Fig. 11. When the electrochemical reactions take place, Pd is reduced from the electrolyte instantaneously (Figs. 8b and 11a). Initial Pd layer leads to P co-deposition and HER, noting that P can be incorporated only by induced deposition. The hydrogen bubbles, outcome of HER, remain longer on Cu substrate than on PdNiP electrodeposits. This fact suggests that the formation of nanopores on film surface (Figs. 9a and 11b) could be caused by a large number of small hydrogen bubbles on Cu substrate at the initial stage. These bubbles grow even bigger, until the surface tension and the stress between bubbles and electrodeposits are too large to keep them (Figs. 9b and 11c). Surface was gradually covered by such inhomogeneous structures as deposition continues. Ultimately, the deposition system saturates and exhibits a diffusive nodular morphology (Figs. 9d and 11d). We further discuss the composition fluctuation during electrodeposition. Once deposition takes place, the films are Pd-dominant and HER occurs simultaneously. As electrochemical reaction continues, the pH value near cathode rises because of the proton depletion. Due to high pH value in local, Pd reduction is accompanied by Ni reduction. The system saturates when HER and metal deposition process reach equilibrium state. In $Pd_{40}Ni_{40}P_{20}$ electrolyte, this behavior leads to designed contents of Pd, Ni, and P.

Conclusions

This paper proposed a $Pd_{40}Ni_{40}P_{20}$ electrodeposition technique with reproducibility of 80%. Current efficiency of this technique is about 15%. Film composition is insensitive to bath composition, but it is sensitive to pH value. At the initial stage, Pd is reduced preferentially, leading to HER and P co-deposition. HER tends to occur at the scratches of Cu substrate, resulting in nanopores on film surface. Film composition saturates after about 60 s, and the growing surface is characterized by diffusive nodular structure. Reduction behavior of $Pd_{40}Ni_{40}P_{20}$ electrolyte is similar to PdP electrolyte and differs from NiP electrolyte. It initiates at −0.45 V, followed by a reduction peak near −0.64 V, and reaches diffusion-limited current region after −1.10 V. $Pd_{40}Ni_{40}P_{20}$ galvanostatic electrodeposition at the current density of 12.5 mA/cm^2 is steady-state reaction-rate controlled and could be regarded as Pd-induced PdNiP co-deposition accompanying with HER.

Acknowledgments The authors thank Prof. Chan Siew Hwa at Nanyang Technological University for fruitful suggestions. Financial support from the National Natural Science Foundation of China (grant nos. 50341032, 50425102, 50601021, 50701038, and 60776014), the Ministry of Education of China (Program for Changjiang Scholars and the Research Fund for the Doctoral Program of Higher Education), Zhejiang University-Helmholtz cooperation fund and Zhejiang University is gratefully acknowledged.

References

1. Maitrepierre PL (1969) J Appl Phys 40:4826
2. Chen H-S (1974) Acta Metall 12:505
3. Drehman AJ, Greer AL, Turnbull D (1982) Appl Phys Lett 41:716
4. Kui HW, Greer AL, Turnbull D (1984) Appl Phys Lett 45:615
5. Ellison CJ, Torkelson JM (2003) Nat Mater 2:695
6. Backer RG, Palumbo TA (1993) Plat Surf Finish 63:70
7. Nam S-E, Lee K-H (2000) J Membrane Sci 170:91
8. Grdeń M, Czerwiński A (2008) J Solid State Electrochem 12:375
9. Lee W-J, Pyun S-I, Yang T-H, Kim J-D, Ho Y, Kim H-G (1997) J Solid State Electrochem 1:120
10. Shobha T, Aravinda CL, Bera P, Devi LG, Mayanna SM (2003) Mater Chem Phys 80:656
11. Daly BP, Barry FJ (2003) Int Mater Rev 48:326
12. Podestá JJ, Piatti RCV (1997) Int J Hydrogen Energy 22:753
13. Swathirajan S, Mikhail YM (1989) J Electrochem Soc 136:2188
14. Ordine AP, Díaz SL, Margarit ICP, Mattos OR (2004) Electrochim Acta 49:2815
15. Bouanani M, Cherkaoui F, Cherkaoui M, Belcadi S, Fratesi R, Roventi G (1999) J Appl Electrochem 29:1171
16. Luborsky FE (ed) (1983) Amorphous metallic alloys. Butterworth, London, p 483
17. Liu Y-M, Sung Y, Chen T-T, Wang H-T, Ger M-D (2007) Mater Chem Phys 106:399
18. Masaki H, Takashi O, Hidemi N, Shozo M (1992) JP19900243481, Japan
19. Kawashima A, Hashimoto K (1982) In: Masumoto T, Suzuki K (eds) Proc 4th Int Conf. Rapidly Quenched Metals. The Japan Institute of Metals, Sendai, p 1427
20. Breneer A, Couch D, Williams E (1950) J Res Natl Bur Stand 44:109
21. Robertis ED, Neves RS, Abrantes LM, Motheo AJ (2005) J Electroanal Chem 581:86
22. Ikeda Y, Nawafune H, Mizumoto S, Sasaki M, Nagatani A, Nishimori A, Yamaguchi K, Uchida E, Okada T (2001) Int J Adhes Adhes 21:233
23. Xiao Y-K, Yu G, Yuan J, Wang J-Y, Chen Z-Z (2006) Electrochim Acta 51:4218
24. Robinson JW (ed) (1974) Handbook of spectroscopy. CRC, Cleveland
25. Alamgir FM, Jain H, Miller AC, Williams DB, Schwarz RB (1999) Philos Mag B 79:239
26. Bulter JN (ed) (1998) Ionic equilibrium. Wiley, New York

27. Harris TM, Wilson JL, Bleakley M (1999) J Electrochem Soc 146:1461
28. Harris TM, Wilson JL (1996) J Electrochem Soc 143:3918
29. Dean JA (ed) (1999) Lange's handbook of chemistry, 15th edn. McGraw-Hill, New York, p 8.93
30. Harris TM, Dang QD (1993) J Electrochem Soc 140:81
31. Zeller RL III, Landau U (1992) J Electrochem Soc 139:3464
32. Bard AJ (1976) Encyclopedia of Electrochemistry of the Elements, vol. 6. Marcel Dekker, New York, p 259
33. Wen S, Corderman RR, Seker F, Zhang A-P, Denault L, Blohm ML (2006) J Electrochem Soc 153:C595
34. Yang Q-Q, Fang B-L, Tong Y-X (ed) (2005) *Appl Electrochem*. Zhongshan University, Guangzhou, p 86
35. Macdonald DD (ed) (1977) Transient technique in electrochemisty. Plenum, New York
36. Delahay P, Berzins T (1953) J Am Chem Soc 75:2486
37. Wen S, Szpunar JA (2005) Electrochim Acta 50:2393